Brazilian Journal of Physics (2024) 54:87
https://doi.org/10.1007/s13538-024-01467-1

SOCIEDADE BRASILEIRA DE FÍSICA

CONDENSED MATTER

Evaluation of the Microstructure and Magnetic Properties of Amorphous $Co_{62}Nb_{32}B_6$ Alloy Produced by Mechanical Alloying

Luciano Nascimento[1] · Elvia Leal[1] · Adriano Lima da Silva[1] · Ana Cristina Figueiredo de Melo Costa[1]

Received: 1 September 2023 / Accepted: 8 April 2024 / Published online: 16 April 2024

Abstract

This work aims to synthesize the alloy $Co_{62}Nb_{32}B_6$ through a wet-route mechanical alloying using a planetary ball mill. A disc rotation per minute and a ball/powder weight ratio of 350 rpm and 20:1 were used, with a grinding time of 15 h, respectively. The characterization of the $Co_{62}Nb_{32}B_6$ alloy was performed by X-ray diffraction (XRD), examined by scanning electron microscope-energy-dispersive X-ray spectroscopy (SEM–EDS), thermoanalytical techniques (TGA/DTA), vibrating sample magnetometer (VSM), and confirmed by the BET method type IV isotherms with a hysteresis loop for mesoporous materials. The results indicated the evolution of the amorphous phase in the $Co_{62}Nb_{32}B_6$ composition through the mechanical alloying process and exhibited good soft magnetic properties with the addition of the B metalloid element and their excellent unique ferromagnetic properties. Through thermoanalytical analysis (TGA/DTA), it was shown that at higher temperatures, oxidation with a significant increase in mass gain of 19.69% at 865 °C, probably due to the contribution of B in the evolution stability thermal and magnetic in the amorphous phase, respectively. This suggests that the newly developed high-performance amorphous alloy $Co_{62}Nb_{32}B_6$ has great application potential.

Keywords Amorphous alloy $Co_{62}Nb_{32}B_6$ · Amorphous phase · Mechanical alloying (MA)

1 Introduction

Since the first amorphous alloy Au–Si was synthesized in the 1960s by Pol Duwez, amorphous alloys have attracted much attention due to their unique properties compared to their crystalline counterparts [1]. Amorphous alloys, with short-range ordered and long-range disordered atomic structures, have recently attracted increasing attention as advanced functional materials [2]. Therefore, an amorphous alloy exhibits unique magnetic properties, good mechanical behavior, and high corrosion resistance compared to other crystalline alloys or pure metals [3]. Amorphous alloys composed of transition metals (such as Co, Fe, Mn, and Ni) and metalloids (such as B, Si, P, and C) favor thermal stability and the soft magnetic behavior of alloys [4, 5]. Additionally, they have the highest compressive yield strength measurements. The magnetic behavior of Co-based alloys is also remarkable due to their high permeability, good soft magnetic characteristics, zero magnetostriction, large magneto-impedance, exceptionally low coercive force, and excellent corrosion resistance [6, 7]. Amorphous alloys have a wide range of applications such as telecommunications [8], computers [9], catalytic supports for the petrochemical industry [10], high-power electrical transformers [11], hydrogen storage [12], metallic biomaterials [13], aerospace [14], marine, and aviation [15].

The synthesis of Co-based magnetic amorphous alloys has attracted attention due to their enormous potential in magnetic applications [16]. Amorphous ferromagnetic Co-based alloys are being developed for motors [17], electrical transformers [18], switching power supplies [19], sensors [20], and other electrical energy conversion devices [21]. Amorphous alloys have been produced via a series of

✉ Luciano Nascimento
luciano.uepb@gmail.com

Elvia Leal
elvialeal@gmail.com

Adriano Lima da Silva
adrianolimsilva@hotmail.com

Ana Cristina Figueiredo de Melo Costa
ana.costaf@ufcg.edu.br

[1] Laboratory of Synthesis of Ceramic Materials – LabSMaC, Academic Unit of Materials Engineering, Federal University of Campina Grande-UFCG, Av. Aprígio Veloso, 882 - Bodocongó, Campina Grande, PB CEP:58429-900, Brazil

techniques such as the melt-spinning method [22], gas atomization (GA) [23], plasma processing [24], and mechanical alloying (MA) [25]. Among these, mechanical alloying (MA) is a peculiar processing technique that can produce a variety of alloys including amorphous [26], quasicrystalline, and high entropy [27, 28]. The advantage of this method is that the powder production capacity is large and the process parameters are easy to control. In this study, we report the preparation of $Co_{62}Nb_{32}B_6$ (wt.%) amorphous powder via a wet route mechanical alloying. The milling time of 15 h was required to effect the amorphization necessary to obtain the amorphous alloy $Co_{62}Nb_{32}B_6$ (wt.%). The evolution of the amorphous powder morphology, microstructure, thermal stability, and soft magnetic properties was investigated and discussed.

2 Exprimental Procedures

Elemental powders (99.9 wt%, from Êxodo Científica – LTDA/Brasil) of Co and B. The Nb powder was donated by Companhia Brasileira de Metalurgia e Mineração (CBMM). The nominal composition of $Co_{62}Nb_{32}B_6$ powder as mechanically alloyed (MA) using a planetary ball mill (Fritsch Pulverisette 5) under an argon atmosphere. The ball-to-powder weight ratio was maintained at 20:1, and the milling speed was set at 350 rpm. The milling process was carried out with hardened stainless-steel balls and vials, containing seven balls (12 mm diameter), for a total milling time of 15 h. Ethyl alcohol (C_2H_6O), from Chemicals Carvalhaes/Rio Grande do Sul/Brazil, was used as a process control agent (PCA) to control the morphology of the homogenized powder. X-ray diffraction measurements (XRD) were performed using a BRUKER diffractometer, model D2 Phaser, with copper radiation CuK_α ($\lambda = 1.54056$ Å), a sweep step of 0.016 s^{-1}, and a time of 5 s, at 40 kV and 30 mA in a 2θ range from $10° \leq 2\theta \leq 80°$. The morphology and chemical compositions of the MA powders were analyzed by scanning electron microscopy (SEM) with energy-dispersive X-ray microanalysis (EDS) using VEGA 3 equipment, from TESCAN, operating at 30 kV with a magnification of 100 kx. Thermogravimetric analysis (TGA-DTA) of the amorphous alloy $Co_{62}Nb_{32}B_6$ was performed, using a SHIMADZU DTG-60H analyzer with a heating rate of 10°Cmin^{-1}, starting from ambient temperature to 1000 °C, under a nitrogen atmosphere with a gas flow of 50 mLmin^{-1} and 10 mg of sample in an alumina crucible. Textural analysis was conducted using a Quantachrome NOVA 2200E BET surface area and pore size analyzer, model Autosorb IQ, to obtain adsorption/desorption isotherms of the amorphous alloy $Co_{62}Nb_{32}B_6$. The magnetic property parameters of the milled powders, including saturation magnetization (M_s), remanence (M_r), coercivity (H_c), and squareness ratio (M_r/M_s), were measured using a Microsense EZ 7 Vibrant Sample Magnetometer (VSM) under magnetic fields up to 2.7 T (i.e., 27 kOe) and at temperatures ranging from 77 to 1000 K.

3 Result and Discussions

In 15 h of milling, the diffractogram was displayed in the 2θ range of 40–50° ($2\theta = 45°$), showing a typical diffuse halo without any obvious diffraction peak corresponding to crystalline phases, indicating a completely amorphous structure as illustrated on the upper right side and highlighted within the dotted red circle in Fig. 1.

Using XRD, Abrosimova et al. observed the same diffuse halo characteristic of an amorphous structure with a peak near $2\theta = 45°$ in the composition of the amorphous alloy type $Al_{87}Ni_8Gd_5$ processed by melt-spinning [29]. Researchers Binh et al. [30] observed a diffuse halo-shaped peak for the Al–Fe-Ni amorphous alloy via mechanical milling [30], supporting the absence of a crystalline phase in the XRD pattern of the amorphous alloy $Co_{62}Nb_{32}B_6$ (see Fig. 1) obtained by MAE.

Micrographs of the SEM/EDS of the powder mixture of $Co_{62}Nb_{32}B_6$ alloy produced both before and after mechanical alloying are shown in Fig. 2.

In 15 h of milling, heterogeneity in particle size and shape is clearly observed. As the milling period increases, intense shear and impact forces are applied to the particles, causing them to break into smaller powders with irregular agglomerate morphologies and wide size variations typical of 50 µm [31]. The size of the powder particles and the irregularity of their shapes tend to decrease with more milling, and the size distribution narrows, as seen in the upper corner of Fig. 2. Following high-intensity mechanical alloying shocks, both the welding and fracture of some particles can be seen in the powder mixture of $Co_{62}Nb_{32}B_6$ alloy, respectively. Additionally, the morphology of the powder particles' irregular agglomerates becomes more uniform and denser [32]. The powder particles become finer by extending the MA process to 15 h, probably as a result of the continued formation of the amorphous phase in their structural makeup (Fig. 2).

During 15 h of milling, the powder particles were refined, and irregular agglomeration occurred, as shown in the enlarged area at the top of the SEM image in Fig. 2. In fact, as milling time increases, the alloy hardens more quickly due to a strong plastic deformation effect. Figure 2 displays the EDS analysis and mapping of the powder obtained after 15 h of milling. Co, Nb, B, and the presence of Au is due to the metallization of the sample present in the initial mixture, according to the EDS analysis. However, the EDS mapping reveals that the powders become inhomogeneous, and distinct clusters of Co and

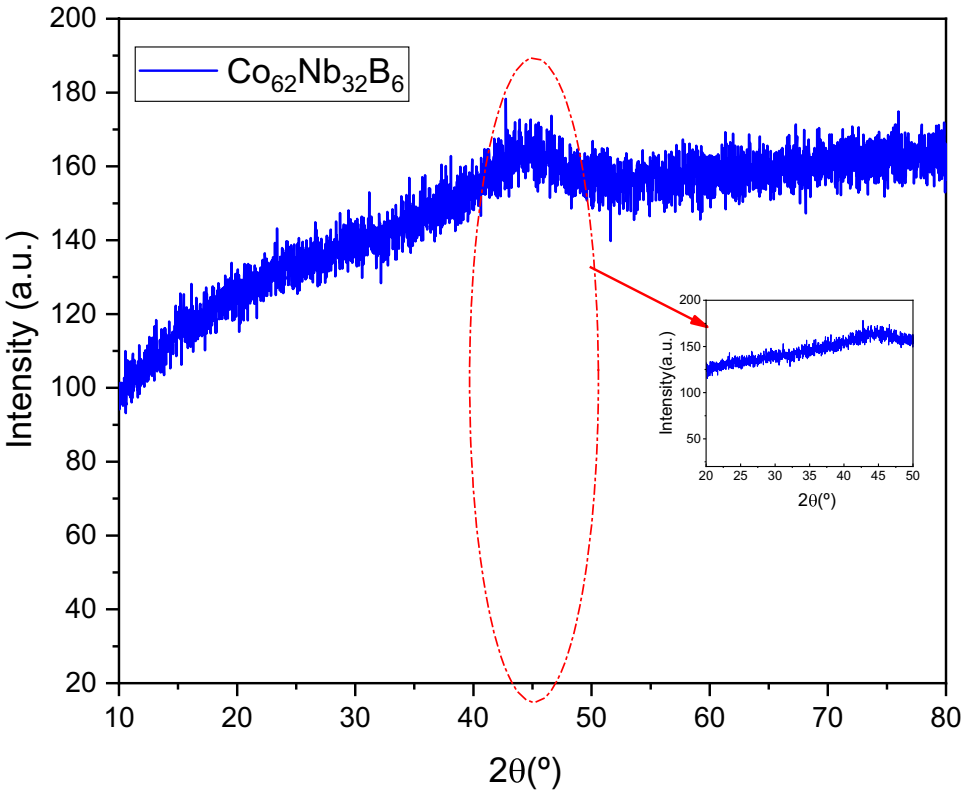

Fig. 1 XRD pattern of $Co_{62}Nb_{32}B_6$ alloy alloy powder

Nb indicate the development of the amorphous phase towards the end result of the powder mixture's milling.

Figure 3 shows the thermal events observed from the superimposed curves of the TGA-DTG curves of $Co_{62}Nb_{32}B_6$ alloy powder obtained by mechanical milling for a period of 15 h and, by heating until 1000 °C under an Ar atmosphere.

According to Fig. 3, it can be said that the $Co_{62}Nb_{32}B_6$ alloy remains an amorphous metallic alloy up to a temperature of approximately 437 °C, where a mass loss of

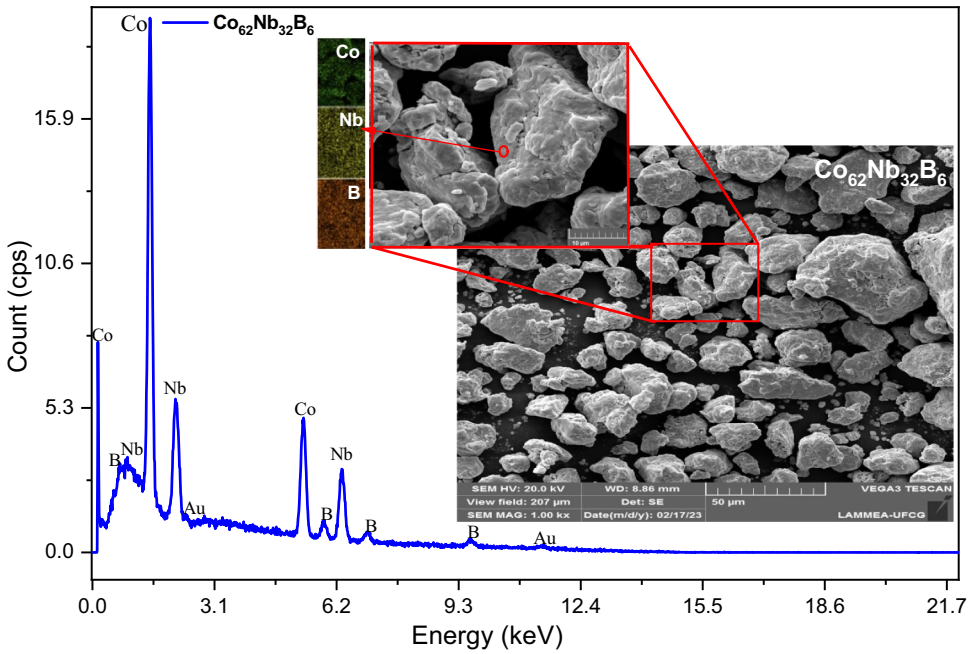

Fig. 2 SEM/EDS micrograph of the $Co_{62}Nb_{32}B_6$ alloy

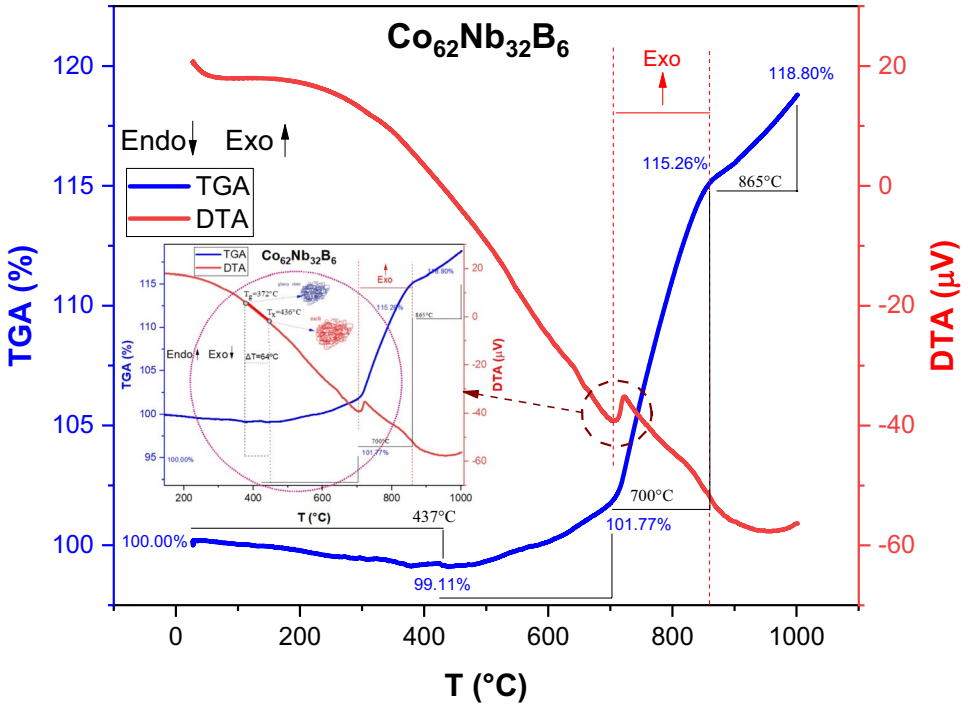

Fig. 3 Thermogravimetric-differential thermal analysis (TGA-DTA) curves of the $Co_{62}Nb_{32}B_6$ alloy

only 0.89% occurs, which is possibly associated with the elimination of moisture and some organic matter present. Subsequently, in the temperature range of 437–700 °C, a small mass gain of 2.66% is observed, showing the beginning of the transformation process from the amorphous phase to the crystalline phase of the metallic alloy [33]. It is also possible to observe that the glass transition temperature (T_g) is about 372 °C and the first crystallization temperature (T_x) is around 436 °C for the amorphous alloy $Co_{62}Nb_{32}B_6$, which corresponds to the supercooled liquid region associated with the endothermic peak, being considered a good indicator for thermal stability. Since the higher value of ΔT causes a growth delay in the grain, i.e., $\Delta T = T_x - T_g = 64$ °C with amorphous alloys/bulk metal glasses (BMG, bulk metal glasses), see the region centered within the dotted circle and enlarged on the right side [34]. Compared with other similar amorphous alloys, the B in the alloy composition effectively increases the crystallization temperature and its thermal stability [35]. From 700 °C, more precisely in the range of 700–865 °C, the DTA curve shows an exothermic peak associated with a significant mass gain of 13.49%, associated with an increase in the crystallines phases, Co_3O_4 and Nb_2O_5 due to oxidation with a significant increase in mass gain we observed at 865 °C [36]. Due to mass gain and multiple steps (oxidation, phase transition, evaporation, and recrystallization) between the the oxides CoO and Co_2O_3 for the Co_3O_4 in an amorphous-like substrate on the outermost layer of the amorphous alloy, the phase transition of the Co_3O_4 crystallizes in a normal spinel structure (space group *Fd3m*) [37]. After temperatures from 875 to 1000 °C, the crystallization process continued with a mass gain of 3.54%, possibly associated with grain growth, leading to a total mass gain of 19.69%.

Figure 4 shows the adsorption/desorption isotherms of N_2 at 77 K for the $Co_{62}Nb_{32}B_6$ alloy after 15 h of milling. The hysteresis loops of the black and red lines represent the adsorption curves (ADS) and desorption (DES).

The illustrated hysteresis loops of the $Co_{62}Nb_{32}B_6$ alloy powder show H3-type hysteresis, indicating slit-shaped pores originating from aggregates of plate-shaped particles. Furthermore, they presented type IV isotherm profiles as illustrated in Fig. 4, suggesting a mesoporous characteristic due to their high density of mesopores, according to the IUPAC classification [38, 39]. The measured specific surface area of the $Co_{62}Nb_{32}B_6$ alloy powder was 3.215 m^2g^{-1}, respectively. These values agree with the results for developed new amorphous alloy catalysts of the Ni–P (R–Ni–P), Ni–Co–B, and Ni–B (P)/SiO_2 type for the Fischer–Tropsch process in catalytic hydrogenation reactions of various organic compounds [40].

The presence of the hysteresis loop indicates that the mesopores also accompany the micropores. This phenomenon was established for activated carbons prepared under low nitrogen flow rates (500 °C) [41]. Thus, it can be concluded that these moderate carbonization conditions contribute to mesopores. It is observed in the isotherms of the amorphous alloy $Co_{62}Nb_{32}B_6$ that the inflection point in the hysteresis occurs around $P/P_o = 0.4–1$, which is typically a characteristic of the strong existence of mesoporos-

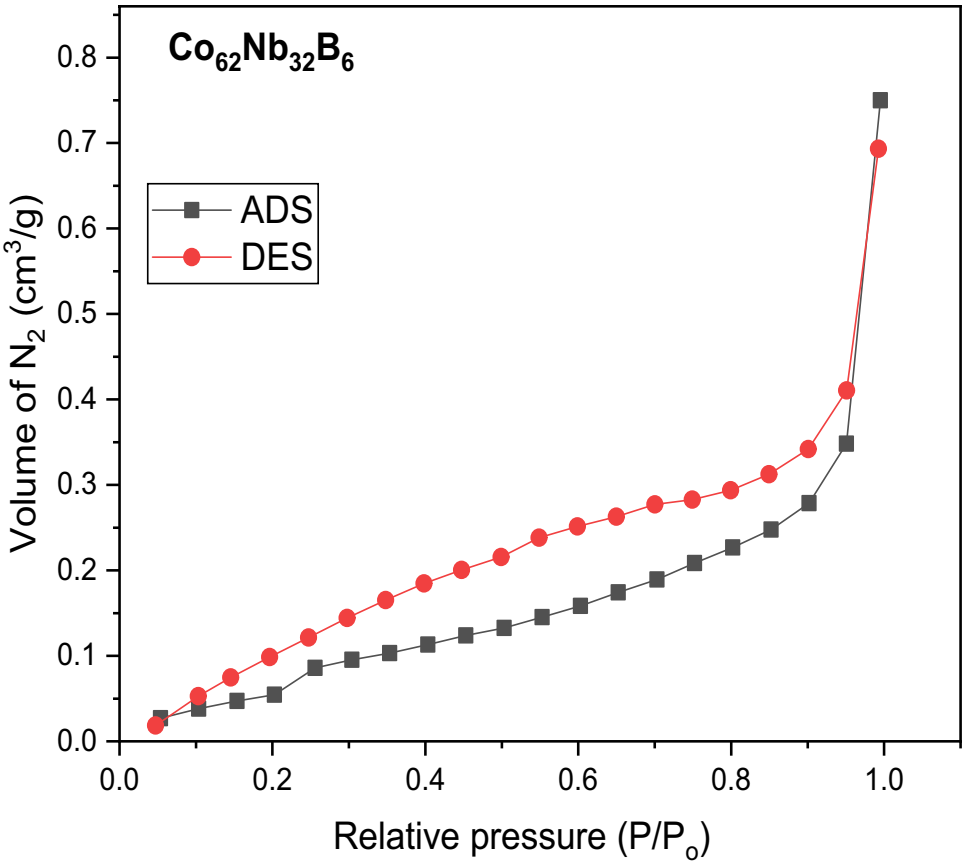

Fig. 4 Adsorption/desorption isotherms of N_2 for $Co_{62}Nb_{32}B_6$ alloy

ity and an adsorption cycle and desorption. Mesoporous phases with medium and large pores were observed in the same range of P/Po = 0.8–1 in the amorphous alloys in which larger pore diameters are as shown in Fig. 4. The hysteresis was caused by the high capillary condensation that occurred in the mesopores [42].

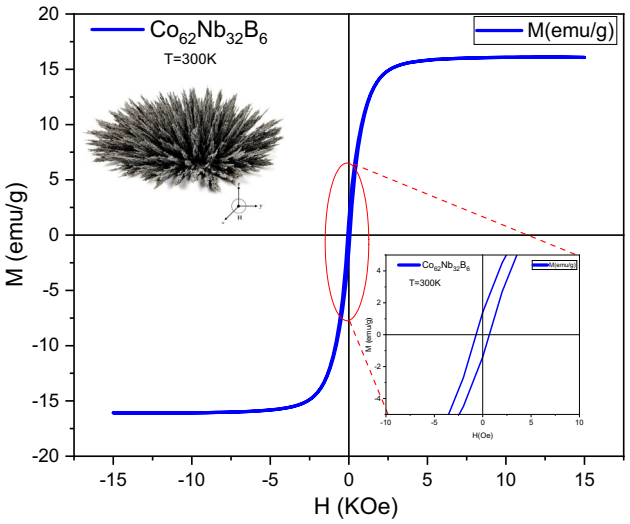

Fig. 5 Hysteresis loop M-H for the $Co_{62}Nb_{32}B_6$ alloy

Figure 5 shows the hysteresis loops M-H for the $Co_{62}Nb_{32}B_6$ alloy, which are typical of soft magnetic ferromagnetic materials.

Hysteresis loop M-H of amorphous alloy $Co_{62}Nb_{32}B_6$ is the estimated value of saturation magnetization $M_s = 16.08$ emu/g, remanent magnetization $M_r = 1.40$ emu/g and a coercive field $H_c = 0.069$ kOe, respectively. During the 15 h of milling, the saturation magnetization decreases to an average value of $M_s = 16.08$ emu/g at the end of milling due to the increase in the amorphous phase volume fraction [43]. Indeed, if the grain sizes are small enough, the structural distortions associated with the surfaces/interfaces reduce the magnitude of the saturation magnetization owing to the deviation of interatomic spacings in the interfacial regions [44]. It is observed that the saturation remanence ratio (M_r/M_s) is 0.087, which is much lower than 0.1 [45]. The remanence-to-saturation ratio, M_r/M_s, is an important magnetic parameter in determining magnetic energy [46]. The variation of the M_r/M_s ratio as a function of milling time is shown in Fig. 5.

Since both the M_r/M_s and the H_c parameters are structurally sensitive, their trends during processing time are almost identical. Therefore, the variations in the M_r/M_s ratio are mainly due to processing conditions, and their explanation is related to the microstructural changes that

the metallic system undergoes during mechanical alloying (MA) [47]. As shown in Fig. 5, the M_r/M_s ratio increases as a function of milling time, indicating a decrease in grain size. The final ratio value obtained of about 0.087, i.e., multi-domains ($M_r/M_s \ll 0.1$) during 15 h of milling, suggests that small magnetic particles are typically single Bloch wall in magnetic domains [48]. In general, the ratio (M_r/M_s) measures how squared the hysteresis loop (M-H) is and is connected to the intensity of inter-grain interactions. According to the Stoner-Wolfarth model, the reduced remanence in single-domain particles with uniaxial anisotropy is of the order of $M_r/M_s = 0.5$ [49], improving the homogeneity of the α-Co/amorphous dual-phase microstructure and promoting the optimization of soft magnetic properties [50].

4 Conclusions

X-ray diffraction analysis showed the formation of a diffuse halo around $2\theta = 45°$, exhibiting a typical diffuse halo without any obvious diffraction peak corresponding to crystalline phases in the milled powder $Co_{62}Nb_{32}B_6$ alloy after 15 h of mechanical alloying. The SEM/EDS micrograph of the $Co_{62}Nb_{32}B_6$ alloy powder showed smaller powders with irregular agglomerate morphologies and wide size variations typical of 50 µm, where the predominance of Co, Nb, and B is distributed uniformly on the surface area according to the EDS analysis.

The presence of Au is due to the metallization of the sample present in the initial mixture. After heating to temperatures ranging from 875 to 1000 °C, the crystallization process continued with a mass gain of 3.54%, associated with an increase in crystalline phases and possibly grain growth, leading to a total mass gain of 19.69%. The N_2 adsorption–desorption isotherms of the $Co_{62}Nb_{32}B_6$ alloy present a type IV isotherm with a hysteresis loop profile characteristic of type H3 for mesoporous materials. Magnetic properties were estimated with a saturation magnetization value of $M_s = 16.08$ emu/g, remanent magnetization of $M_r = 1.40$ emu/g, and a coercive field of $H_c = 0.069$ kOe for a ferromagnetic material, featuring superior soft magnetic properties and expected to have attractive application prospects. The final ratio value obtained of about 0.087, i.e., multi-domains ($M_r/M_s \ll 0.1$) during 15 h of milling, suggests that small magnetic particles are typically single Bloch wall in magnetic domains.

This manuscript has not been submitted to any previous journal of this journal. The presented work is original and has not been published elsewhere in any form or language.

Acknowledgements The authors wish to thank CAPES for the financial support of this research and Companhia Brasileira de Metalurgia e Mineração (CBMM).

Declarations

Consent to Participate Not applicable.

Consent for Publication All authors have read and consented to the published version of the manuscript.

Conflict of Interest The authors declare no competing interests.

References

1. K. Bobzin, H. Heinemann, M. Erck, O. Stryzhyboroda, S. Vinke, Novel Fe-based amorphous brazing foils in the quinary system Fe–Ni–Cr–Si–B. Adv. Eng. Mater. **26**(4), 2300403 (2024)
2. J. Kang, X. Yang, Q. Hu, Z. Cai, L.M. Liu, L. Guo, Recent progress of amorphous nanomaterials. Chem. Rev. **123**(13), 8859–8941 (2023)
3. C.Y. Liu, Y.X. Zhang, C.Y. Zhang, J. Kang, G. Yuan, R.D.K. Misra, Thermal, magnetic and mechanical behavior of large-sized Fe-based amorphous alloy ribbons by twin-roll strip casting. Intermetallics **132**, 107144 (2021)
4. J. Zhou, J. You, K. Qiu, Advances in Fe-based amorphous/nanocrystalline alloys. J. Appl. Phys. **132**(4) (2022)
5. I. Permyakova, A. Glezer, Mechanical behavior of Fe-and Co-based amorphous alloys after thermal action. Metals **12**(2), 297 (2022)
6. X. Liang, Y. Li, F. Bao, Z. Zhu, H. Zhang, W. Zhang, Roles of Y and Fe contents on glass-forming ability, thermal stability, and magnetic properties of Co-based Co–Fe–Y–B bulk metallic glasses. Intermetallics **132**, 107135 (2021)
7. M.G. Nematov, I. Baraban, N.A. Yudanov, V. Rodionova, F.X. Qin, H.X. Peng, L.V. Panina, Evolution of the magnetic anisotropy and magnetostriction in Co-based amorphous alloys microwires due to current annealing and stress-sensory applications. J. Alloy. Compd. **837**, 155584 (2020)
8. F. Luo, F. Sun, K. Li, F. Gong, X. Liang, X. Wu, J. Ma, Ultrasonic assisted micro-shear punching of amorphous alloy. Materials Research Letters **6**(10), 545–551 (2018)
9. N. Xu, Y. Shi, Y. He, Q. Shao, A deep-learning potential for crystalline and amorphous Li–Si alloys. J. Phys. Chem. C **124**(30), 16278–16288 (2020)
10. Z. Li, B. Li, M. Yu, C. Yu, P. Shen, Amorphous metallic ultrathin nanostructures: a latent ultra-high-density atomic-level catalyst for electrochemical energy conversion. Int. J. Hydrogen Energy **47**(63), 26956–26977 (2022)
11. S. Zhang, D. Chen, B. Bai, Study of a high-power medium frequency transformer using amorphous magnetic material. Symmetry **14**(10), 2129 (2022)
12. L.J. Huang, H.J. Lin, H. Wang, L.Z. Ouyang, M. Zhu, Amorphous alloys for hydrogen storage. J. Alloy. Compd. **941**, 168945 (2023)
13. M. Biały, M. Hasiak, A. Łaszcz, Review on biocompatibility and prospect biomedical applications of novel functional metallic glasses. J. Funct. Biomater. **13**(4), 245 (2022)
14. H. He, X. Yuan, W. Liu, Application direction of amorphous and nanocrystalline alloy materials and the evaluation of venture capital value. Ferroelectrics **581**(1), 17–31 (2021)

15. L. Wu, Z. Zhou, X. Zhang, Y. Liu, G. Wang, K. Zhang, Characterization of microstructure and passive film difference of FeCr-MoCB amorphous coatings affected by feedstock specific surface area. Surf. Coat. Technol. **457**, 129333 (2023)
16. X.L. Zhang, Y. Wu, R.R. Liu, J.H. Liu, H.T. Zhou, A study of crystallization behavior and magnetic property of Co-based alloy. J. Non-Cryst. Solids **619**, 122562 (2023)
17. H. Cui, B. Dong, Y. Xing, Y. Cheng, L. Wang, S. Zhou, Soft magnetic properties of FeCoSiBC amorphous alloys with high saturation magnetization. J. Mater. Sci. Mater. Electron. **34**(26), 1801 (2023)
18. M. Nazmunnahar, S. Simizu, P.R. Ohodnicki, S. Bhattacharya, M.E. McHenry, Finite-element analysis modeling of high-frequency single-phase transformers enabled by metal amorphous nanocomposites and calculation of leakage inductance for different winding topologies. IEEE Trans. Magn. **55**(7), 1–11 (2019)
19. X. Qi, J. You, J. Zhou, K. Qiu, X. Cui, J. Tian, B. Li, A review of Fe-based amorphous and nanocrystalline alloys: Preparations, applications, and effects of alloying elements. Phys. Status Solidi (a) **220**(14), 2300079 (2023)
20. A. Dzhumazoda, L.V. Panina, M.G. Nematov, A.A. Ukhasov, N.A. Yudanov, A.T. Morchenko, F.X. Qin, Temperature-stable magnetoimpedance (MI) of current-annealed Co-based amorphous microwires. J. Magn. Magn. Mater. **474**, 374–380 (2019)
21. Y. Nykyruy, S. Mudry, Y. Kulyk, A. Borisyuk, Magnetic properties and nanocrystallization process in Co–(Me)–Si–B amorphous ribbons. Appl. Nanosci. **13**(7), 5239–5249 (2023)
22. X. Jia, B. Zhang, W. Zhang, Y. Dong, J. Li, A. He, R.W. Li, Direct synthesis of Fe-Si-B-CCu nanocrystalline alloys with superior soft magnetic properties and ductile by melt-spinning. J. Mater. Sci. Technol. **108**, 186–195 (2022)
23. Y.T. Shi, W.Y. Lu, W.H. Sun, S.D. Zhang, B.J. Yang, J.Q. Wang, Pressure-dependent microstructure evolution of Fe-based amorphous alloy powders via high-pressure gas atomization. J. Alloy. Compd. **920**, 166038 (2022)
24. W. Zhang, H. Wei, Z. Li, Q. Shan, F. Zhang, Interfacial bonding, corrosion, and wear behavior of Zr-based amorphous ($Zr_{41.2}Ti_{13.8}Cu_{12.5}Ni_{10}Be_{22.5}$) alloy coatings prepared by plasma spraying technique. Surface Coat. Technol. **470**, 129818 (2023)
25. B. Avar, A.K. Chattopadhyay, T. Simsek, T. Simsek, S. Ozcan, B. Kalkan, Synthesis and characterization of amorphous-nanocrystalline $Fe_{70}Cr_{10}Nb_{10}B_{10}$ powders by mechanical alloying. Appl. Phys. A **128**(6), 537 (2022)
26. A. Yakin, T. Simsek, B. Avar, T. Simsek, A.K. Chattopadhyay, A review of soft magnetic properties of mechanically alloyed amorphous and nanocrystalline powders. Emerg. Mater. **6**(2), 453–481 (2023)
27. H.V. Nguyen, N.B. Do, T.H.O. Nguyen, C.S. Nguyen, V.T. Trinh, H.T. Le, A.M. Jorge Junior, Synthesis and magnetic properties of Al–Cu–Fe quasicrystals prepared by mechanical alloying and heat treatment. J. Mater. Res. **38**(3), 644–653 (2023)
28. M.A. Karimi, M. Shamanian, M.H. Enayati, M. Adamzadeh, M. Imani, Fabrication of a novel magnetic high entropy alloy with desirable mechanical properties by mechanical alloying and spark plasma sintering. J. Manuf. Process. **84**, 859–870 (2022)
29. G. Abrosimova, V. Chirkova, E. Pershina, N. Volkov, I. Sholin, A. Aronin, The effect of free volume on the crystallization of $Al_{87}Ni_8Gd_5$ amorphous alloy. Metals **12**(2), 332 (2022)
30. D.N. Binh, N.T.H. Oanh, N.H. Viet, Al-Fe-Ni metallic glasses via mechanical alloying and ıts consolidation. Appl. Sci. **12**(20), 10561 (2022)
31. H. Yaykasli, B. Avar, M. Panigrahi, M. Gogebakan, H. Eskalen, Investigation of the microstructural, morphological, and magnetic properties of mechanically alloyed $Co_{60}Fe_{18}Ti_{18}Si_4$ powders. Arab. J. Sci. Eng. **48**(1), 845–854 (2023)
32. M. Shan, C. Zhang, N. Wang, L. Zhang, W. Li, X. Yin, Improvement in wear resistance of laser-clad Fe–Cr–Mo–B–C-(TiC) amorphous-nanocrystalline coating. Vacuum **207**, 111676 (2023)
33. J.H. Park, J.I. Kim, Y. Shinohara, T. Hagio, N. Umehara, R. Ichino, Super hardening of FeW alloy plating by phase transformation of amorphous to metal carbides-dispersed nanocrystalline alloys and application as promising alternative for hard chromium plating. Surf. Coat. Technol. **477**, 130388 (2024)
34. A. Kuś, W. Pilarczyk, A. Małachowska, A. Ambroziak, P. Gębara, Investigation of mechanical and magnetic properties of Co-based amorphous powders obtained by atomization. Materials **14**(23), 7357 (2021)
35. S. Lu, J. Zhang, H. Duan, Effects of B substitution for P on structure and magnetic properties of FePB amorphous alloys by first-principle investigation. Intermetallics **149**, 107674 (2022)
36. B.D. Bankar, K. Ravi, S. Subramanian, A.V. Biradar, Niobium oxide supported on cubic spinel cobalt oxide as an efficient heterogeneous catalyst for the synthesis of imines via dehydrogenative coupling of amines and alcohols. Catal. Lett. **152**(12), 3733–3746 (2022)
37. Y. Nykyruy, S. Mudry, Y. Kulyk, V. Prunitsa, A. Borysiuk, Magnetic properties and nanocrystallization behavior of Co-based amorphous alloy. Phys. Chem. Solid State **24**(1), 106–113 (2023)
38. K.A. Cychosz, M. Thommes, Progress in the physisorption characterization of nanoporous gas storage materials. Engineering **4**(4), 559–566 (2018)
39. C. Schlumberger, M. Thommes, Characterization of hierarchically ordered porous materials by physisorption and mercury porosimetry—a tutorial review. Adv. Mater. Interfaces **8**(4), 2002181 (2021)
40. J.F. Deng, H. Li, W. Wang, Progress in design of new amorphous alloy catalysts. Catal. Today **51**(1), 113–125 (1999)
41. J. Serafin, K. Kiełbasa, B. Michalkiewicz, The new tailored nanoporous carbons from the common polypody (Polypodium vulgare): The role of textural properties for enhanced CO_2 adsorption. Chem. Eng. J. **429**, 131751 (2022)
42. C.F. Toncón-Leal, J. Villarroel-Rocha, M.T.P.D. Silva, T.P. Braga, K. Sapag, Characterization of mesoporous region by the scanning of the hysteresis loop in adsorption–desorption isotherms. Adsorption **27**(7), 1109–1122 (2021)
43. S. Souilah, S. Alleg, C. Djebbari, R. Bensalem, J.J. Sunol, Magnetic and microstructural properties of the mechanically alloyed $Fe_{57}Co_{21}Nb_7B_{15}$ powder mixture. Mater. Chem. Phys. **132**(2–3), 766–772 (2012)
44. R. Daly, N. Khitouni, M.L. Escoda, N.L. Isern, S.M. Juan Jose, J.M. Greneche, M. Khitouni, Microstructure, magnetic and Mössbauer studies of mechanically alloyed FeCoNi nanocrystalline powders. Arab. J. Sci. Eng. **46**, 5633–5643 (2021)
45. Z. Li, F. Wang, C. Zhao, Y. Liao, M. Gao, H. Zhang, Microstructural evolution and enhanced magnetic properties of $FeCoNiZr_x$ medium entropy alloy films. J. Alloy. Compd. **971**, 17264 (2024)
46. Z. Msetra, N. Khitouni, A. Alsawi, M. Khitouni, V. Optasanu, J.J. Suñol, M. Chemingui, Structural, microstructural, and magnetic properties of nanocrystalline-amorphous Fe–Co–Ta–B alloy processed by high-energy mechanical alloying. J. Market. Res. **26**, 8934–8943 (2023)
47. M. Triki, H. Mechri, H. Azzaz, M. Azzaz, Characterization of nanostructured magnetic alloy based on Ni-Co-Mn produced by mechanical synthesis. J. Magn. Magn. Mater. **541**, 168514 (2022)

48. A. Chebli, M. Cesnek, A. Djekoun, J.J. Sunol, D. Niznansky, Synthesis, characterization and amorphization of mechanically alloyed $Fe_{75}Si_{12}Ti_6B_7$ and $Fe_{73}Si_{15}Ti_5B_7$ powders. J. Mater. Sci. **57**(26), 12600–12615 (2022)
49. X. Xu, L. Jin, T. Wen, Y. Liao, X. Tang, H. Zhang, Z. Zhong, Effects of substrate annealing on uniaxial magnetic anisotropy and ferromagnetic resonance frequency of $Ni_{80}Fe_{20}$ films deposited on self-organized periodically rippled sapphire substrates. Vacuum **186**, 110047 (2021)
50. D.W. Zhang, Y. Zhang, Y.F. Cai, B.W. Zang, F. Zhao, Y.C. Wang, R. Umetsu, Z.Z. Li, X. Tong, J.T. Huo, S.L. Che, J.Q. Wang, Magnetic properties evaluation of Fe-based amorphous alloys synthesized via spark plasma sintering. J. Non-Cryst. Solids **613**, 122373 (2023)